RSC Advances

PAPER

View Article Online
View Journal | View Issue

Cite this: *RSC Adv.*, 2025, **15**, 2618

Effect of polishing on the morphology of Zircaloy-4 nanostructure: formation of a novel hexagonal nanoscale pattern†

Ghafar Ali, *[a] Maaz Khan, [a] Shahzad Anwar,[b] Khalid M. Alotaibi,[c] Kashif Safeen, *[d] Akif Safeen[e] and Sung Oh Cho *[f]

Zircaloy-4 (Zr-4) is widely used as the cladding material in nuclear power plants (NPPs) due to its excellent corrosion resistance and low neutron absorption cross-section. Under Loss of Coolant Accident (LOCA) conditions, oxidation of Zr-4 can compromise the safety of the NPPs by accelerating hydrogen production. Therefore, enhancing the oxidation resistance of Zr-4 is a critical research focus. Surface modification through a facile method offers a promising approach to address this issue. This study explores the impact of chemical, mechanical, and electropolishing (EP) pre-treatments on Zr-4 morphology before and after anodization. EP conducted in ethylene glycol monobutyl ether–perchloric acid electrolyte produced a mirror-like surface finish with hexagonal nanopattern formation under optimized conditions, as revealed by SEM studies. Anodization of the patterned surface in a glycerol-based electrolyte resulted in a hybrid (nanoporous and nanotubular) structure, unlike the nanotubular-only morphology observed in the chemically or mechanically polished samples. EDAX and XRD analyses confirmed the formation of ZrO_2. The hexagonal nanopattern generated by EP suppressed the dissolution of the nanotube during anodization, resulting in a hybrid nanostructure. Additionally, the chemical polishing of EP-treated Zr-4 in $HF : HNO_3 : H_2O$ generated a porous particulate structure due to selective etching. This work demonstrates that the surface pre-treatment significantly influences the morphology of anodized Zr-4 nanostructures and suggests the potential use of EP in other materials for hexagonal nanopattern generation.

Received 27th May 2024
Accepted 15th January 2025

DOI: 10.1039/d4ra03903c

rsc.li/rsc-advances

1. Introduction

Zircaloy-4 (Zr-4) is an essential zirconium-based alloy primarily used as a cladding material for fuel pellets in nuclear power plants (NPPs) due to its low absorption cross-section (for thermal neutrons) and relatively high anti-corrosion properties.[1–5] Zircaloy-4 cladding tubes serve as a barrier between fuel pellets and nuclear reactor coolant, which prevents the direct interaction of fuel pellets with coolant, thus ensuring the safety of NPPs. During the normal operation of nuclear power reactors, coolant (water) continuously interacts with Zr-4 cladding tubes to reduce the heat generated in fuel pellets due to the nuclear fission reaction. The recent Fukushima NPP accident in Japan grabbed the attention of researchers worldwide in this important field due to public health and safety issues. Oxidation of the Zr-4 cladding tubes due to coolant interaction is crucial regarding nuclear power reactor safety and public health. Oxidation generally deteriorates materials, thus causing accidents like that at Fukushima under LOCA conditions, which trigger the uncontrolled production of hydrogen gas (H_2) from the coolant (water) due to the expedited oxidation reaction. Efforts are being made to improve the present Zr-4 technology in addition to exploring and developing new cladding materials for the safety of NPPs. Our group is trying to improve the existing Zr-4 cladding materials, which are well-mature and have been successfully used in NPPs for decades. Therefore, we reported a simple strategy to enhance the oxidation resistance of Zr-4 cladding material using a facile, fast and cost-effective approach.

Self-organised anodic nanoporous and nanotubular structures have attracted tremendous interest due to their unique morphology, fabrication simplicity, cost-effectiveness, high

[a]*Nanomaterials Research Group (NRG), Physics Division, PINSTECH, Nilore, Islamabad 44000, Pakistan. E-mail: ghafarali@kaist.ac.kr; Fax: +92-51-9248808; Tel: +92-51-924801*

[b]*Physics Department, Islamia College University, Peshawar, KPK, Pakistan*

[c]*Department of Chemistry, College of Science, King Saud University, PO Box 2455, Riyadh 11541, Saudi Arabia*

[d]*Department of Physics, Abdul Wali Khan University Mardan, Pakistan. E-mail: kashifsafeen@awkum.edu.pk*

[e]*Department of Physics, University of Poonch Rawalakot, 12350, AJK, Pakistan. E-mail: akifsafeen@upr.edu.pk*

[f]*Department of Nuclear and Quantum Engineering, Korea Advanced Institute of Science and Technology (KAIST), 291 Daehak-ro, Yuseong-gu, Daejeon 34141, Republic of Korea. E-mail: socho@kaist.ac.kr*

† Electronic supplementary information (ESI) available. See DOI: https://doi.org/10.1039/d4ra03903c

purity, and versatile applications.[6–12] For the first time, our group produced a self-organised nanotubular structure as an oxide layer on the surface of Zr-4 in an ethylene glycol-based electrolyte using anodization.[13] We also tailored Zr-4 nanotubular morphology and obtained a highly ordered hexagonal nanoporous structure on the surface of Zr-4 using the two-step anodization.[14] In another work, we reported that nanotubular or nanoporous structure morphology could be controllably and selectively grown simultaneously on the Zr-4 surface depending on the anodization conditions.[15] Real progress was made when we anodized a long cylindrical Zr-4 cladding tube (in meters) and obtained a homogeneous, highly-ordered nanoporous structure on its surface.[16] The Zr-4 anodic nanoporous structure (surface treated) was employed for corrosion studies at high temperatures in harsh environments.[2] For comparison, the un-anodized (un-treated) Zr-4 sample was also tested under similar conditions of corrosion studies. Interestingly, Zr-4 with an anodic nanoporous structure showed excellent corrosion resistance at high temperatures in air and steam environments compared to the bare (un-anodized) Zr-4 sample. Similarly, in our recent findings on critical heat flux (CHF) experiments of zirconium alloy (Zirclo), we observed enhancement in CHF using mechanically polished and anodized Zirclo samples compared to non-polished and un-anodized samples.[17] These results revealed the importance of the pre-treatment technique (anodization and mechanical polishing) in enhancing the anti-corrosion and CHF properties of Zr-4.

Polishing is one of the oldest pre-treatment techniques widely used in industries for surface finishing materials.[18–22] It is very facile and economical compared to other pre-texturing methods. Pre-texturing techniques have profoundly affected the resulting anodic TiO_2 morphology.[23–26] The surface roughness of materials decreases during mechanical polishing (MP) and electropolishing (EP) in different ways. MP is carried out manually, and a smooth surface is achieved by removing material using SiC abrasive papers of different grit successively (starting from coarse grain to fine grain), followed by alumina (Al_2O_3) slurry for mirror-like finishing. It generally removes scratches, gauges, and surface defects and is considered very laborious. On the other hand, EP is an electrolyte (solution) based technique in which an extremely smooth surface is produced with the help of direct current. It provides good control over the material's surface finishing by tailoring parameters like voltage, current, time, bath temperature, nature, and electrolyte concentration. It is a powerful technique compared to MP, as it can be applied even to complex shaped materials. The effect of surface finishing on the anodic morphologies has been extensively studied for aluminium[27–29] and stainless steel,[30–32] while few reports are also available on Ti.[33,34] Recently, we have reported that EP generated a highly ordered and perfect hexagonal nanopattern on the surface of stainless steel (Sus-304L).[35] Subsequent anodization of the patterned morphology in organic electrolyte produced ideal nanopores on the surface of Sus-304L.[35] Although reports (mostly from our group) are available on the anodization of Zr-4 in various electrolytes under different conditions;[13–17,36–38] however, no work has been conducted to study the effect of different polishing techniques on Zr-4 surface morphology.

The main objectives of this study were to investigate (i) whether the pre-treatment methods are effective for achieving smooth Zr-4 surface with nanopattern formation before anodization like aluminium and stainless steel and (ii) the effect of these pre-treatments on Zr-4 anodic morphology. Before anodization, we carried out CP, MP, and EP of Zr-4 sheets separately and in combination. For the first time, we obtained a novel honeycomb-like hexagonal and highly ordered nanopattern on the surface of Zr-4 with the help of EP only. We proposed a possible mechanism for forming a hexagonal nanopattern with EP. Subsequent anodization of the polished samples was conducted in a glycerol-based electrolyte containing 0.1 M H_2O and 0.1 M NH_4F under similar conditions. Anodization of the Zr-4 sample with nanopattern morphology produced a novel hybrid nanostructure in contrast to the mechanically polished samples. In addition, the effect of MP + CP and EP + CP on the surface morphology of Zr-4 anodic nanostructure was also evaluated.

2. Experimental procedure

2.1 Material and chemicals

KEPCO Nuclear Fuel Ltd Company, South Korea, supplied Zircaloy-4 sheets with 0.7 mm thickness. Ethylene glycol monobutylether (2-butoxyethanol, $C_6H_{14}O_2$), perchloric acid ($HClO_4$, 60% pure), methanol (CH_3OH, 99.8% purity), ammonium fluoride (NH_4F, 99.99% purity), hydrochloric acid (HCl, 35% purity), hydrofluoric acid (HF, 40% pure), nitric acid (HNO_3, 65% purity) were purchased from Sigma-Aldrich, USA. Glycerol ($C_3H_8O_3$, 99.999% extra pure) was obtained from Junsei, Japan. SiC grit papers and alumina slurry were purchased from Struers (Copenhagen, Denmark). Deionized (DI) water was used in all experiments. All chemicals were used in their as-received form without further purification.

2.2 Polishing of Zr-4 sheets

The as-received Zr-4 sheets were cut into the desired sizes for polishing (chemical, mechanical and electrochemical) and anodization. Prior to anodization, Zr-4 sheets were cleaned by sonicating in acetone, isopropyl alcohol, and ethanol each for 3 min. Subsequently, Zr-4 sheets were rinsed with DI water and dried in an air stream at high pressure. The sheets were chemically polished in an electrolyte comprising $HF : HNO_3 : H_2O$ with a volume ratio of 2 : 4 : 1, respectively, for different times (3 and 5 min immersion) at room temperature, as illustrated in Table 1. Chemical polishing was conducted in a glove box under a controlled environment, following a proper protocol due to the toxicity of HF and HNO_3. In ascending order sequence, MP of Zr-4 sheets was carried out on a grinding polisher using SiC papers of different grits (250, 400, 800, 1200, and 4000). MP timing was different at each step depending on the surface smoothness conditions. The scratches-less surface of Zr-4 sheets was achieved after MP at 4000 grit for 15 min. Finally, MP was conducted on a velvet cloth using alumina slurry of various particle sizes (3.0 μm, 0.25 μm, and 0.1 μm) for different time intervals to obtain a smooth, flat surface with a mirror-like finish. EP was performed in two different electrolytes: methanol–per-chloric acid and

Table 1 Process conditions for chemical, mechanical, and electropolishing

Sample name	Time	Conditions
Chemical polishing		
CP-3min-HFHNO$_3$	3 min	HF : HNO$_3$: H$_2$O = 2 : 4 : 1
CP-5min-HFHNO$_3$	5 min	HF : HNO$_3$: H$_2$O = 2 : 4 : 1
Mechanical polishing		
MP-250-10min	10 min	250 grit SiC paper
MP-400-20min	20 min	400 grit SiC paper
MP-800-25min	25 min	800 grit SiC paper
MP-1200-35min	35 min	1200 grit SiC paper
MP-4000-45min	45 min	4000 grit SiC paper
Electropolishing		
EP-MeOH-5V-1min	1 min	Methanol–perchloric acid, 5 V, −1 °C
EP-MeOH-10V-30s	0.5 min	Methanol–perchloric acid, 10 V, −1 °C
EP-MeOH-10V-1min	1 min	Methanol–perchloric acid, 10 V, −1 °C
EP-MeOH-10V-3min	3 min	Methanol–perchloric acid, 10 V, −1 °C
EP-EG-50V-3°C-30min	30 min	Ethylene glycol–perchloric acid, 50 V, −5 °C
EP-EG-50V-3°C-1min	1 min	Ethylene glycol–perchloric acid, 50 V, −3 °C
Anodization		
AN-50V-2h	2 h	Glycerol-based electrolyte, 0.3 wt% NH$_4$F, 0.2 wt% DI water, 50 V, room temperature

ethylene glycol monobutyl ether–perchloric acid electrolytes in a 4 : 1 volume ratio at constant voltage (5, 10, and 50 V) for different times (30 seconds, 1 min, and 30 min) at different temperature (−1 °C, −5 °C, and 3 °C) using programmable DC power supply (ODA, OPS-3003, Korea). During EP, the electrolyte temperature was maintained uniformly using a chiller with a unique electrochemical set-up. EP of Zr-4 sheets was carried out using a specially designed two-electrode system with platinum gauze (15 × 25 × 0.2 mm^3) or O-ring shaped Cu as the counter electrode and Zr-4 sheet as the working electrode. The electrolyte was stirred continuously during EP to maintain a uniform and homogeneous temperature. Subsequently, after polishing, the samples were washed with ample DI water, cleaned with ethanol and water each for 3 min in an ultrasonic bath, and then dried in the oven at 70 °C. The polished samples were anodized in glycerol-based electrolyte containing 0.3 wt% NH$_4$F and 0.2 wt% DI water at 50 V for 2 h at room temperature. The anodization process was conducted in a two-electrode system with platinum gauze as the counter electrode and the polished Zr-4 sheets as the working electrode. Depending upon the surface conditions obtained through polishing, anodization produced different nanostructured morphologies on Zr-4. A detailed microscopic study of all the samples was carried out with the help of a field emission scanning electron microscope (FESEM; Hitachi S-4800, Tokyo, Japan).

3. Results and discussion

3.1 Mechanical polishing effect on Zr-4 morphology before anodization

A digital picture of the mechanically polished Zr-4 sheet (MP-4000-45min) is depicted in Fig. 1a, which shows that the dull surface of the as-received Zr-4 sheet is converted into a smooth surface with mirror-like shining after MP. The FESEM image in Fig. 1b reveals that the rough surface of the as-received Zr-4 sheet contains some cracks and tiny pores over the whole surface. With the help of MP, these tiny pores and cracks of the sample MP-4000-45min disappeared, and a relatively smooth surface was achieved (Fig. 1c). However, some grains can still be seen on the surface of Zr-4 after MP (high magnification image in the inset). This result shows that MP is beneficial for reducing Zr-4 surface roughness.

3.2 Electropolishing effect on the Zr-4 morphology before anodization

EP is generally considered an effective technique to smooth the rough surface of metals and alloys and is inspired by our recent findings in the case of Sus-304L[35] and Sn,[39,40] where an immaculate and smooth surface with patterned morphology was achieved during EP. Therefore, the same technique was applied to Zr-4 sheets before anodization. Two different electrolytes were used for the EP of the Zr-4 sheet. Digital pictures of the Zr-4 sheets electropolished in methanol–perchloric acid electrolyte at various conditions (see Table 2 for details) are shown in Fig. 2a. This indicates that the Zr-4 surface exposed to the EP electrolyte appeared very bright and shiny compared to the non-polished surface, which was dull and rough. Small bubble formations and some erosion can be seen, which increase with increasing EP timing (i–v). Pitting might be one of the possible reasons for the bubble formation and erosion due to the uneven removal of Zr-4 material by electrolyte during EP due to the non-uniform electric field. This fact can be explained in the following section based on our findings in the case of Zr-4 anodization. Homogeneous, smooth, and uniform Zr-4 surfaces

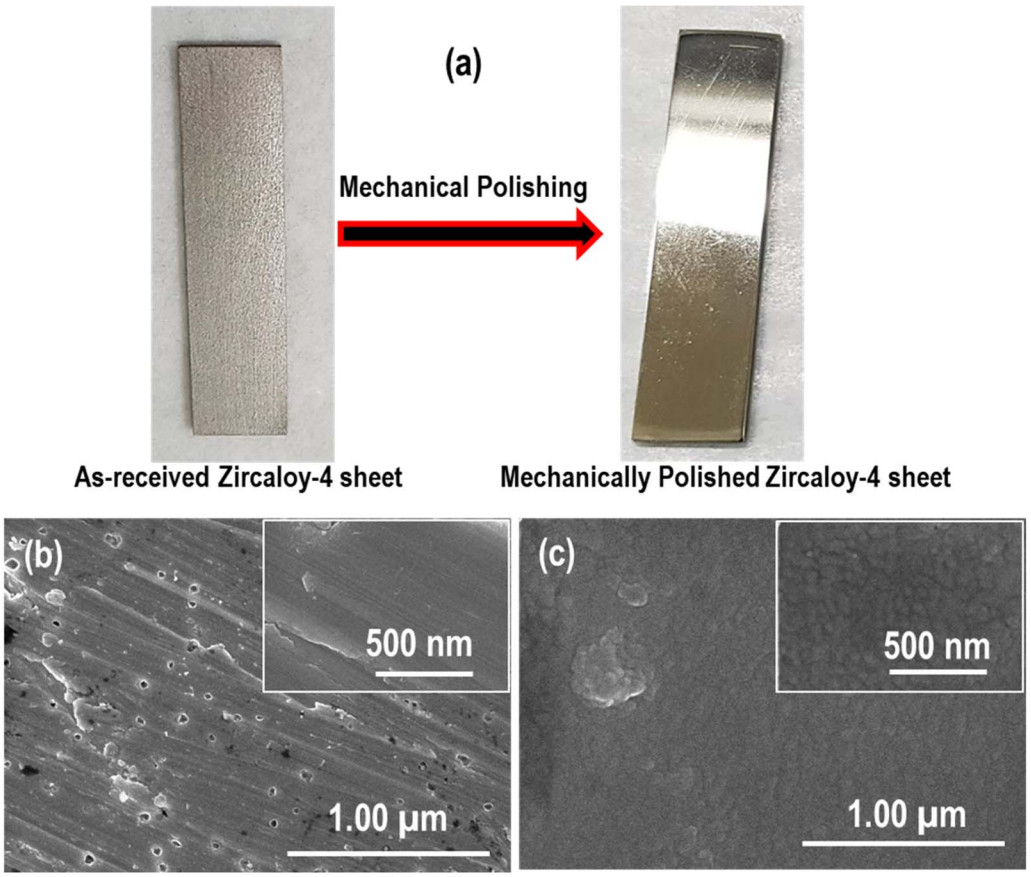

Fig. 1 (a) Digital picture of the as-received and mechanically polished Zr-4 sheet, FESEM images showing the morphology of the (b) as-received Zr-4 sheet, (c) mechanically polished Zr-4 sheet (MP-4000-45min).

were achieved when EP was conducted for 30 seconds and 1 minute at 10 V and 5 V, respectively, at −1 °C (Fig. 2a(i) and (iii)). The reaction during EP was very vigorous and fast; therefore, the EP timing was reduced with increased voltage. It is worth mentioning that EP without electrolyte stirring led to the dissolution of the Zr-4 sheet from a side (Fig. S1a†). This can be ascribed to the non-uniform temperature generated around the anode surfaces due to vigorous and fast chemical reactions. Although EP was carried out in a controlled environment, the local temperature can be increased due to non-uniform etching during EP due to defects, stresses, *etc.* The edge effect might also contribute to this phenomenon.[41] This problem was overcome by continuously stirring the electrolyte during EP to maintain a homogeneous and uniform temperature. Martin *et al.* reported that stirring is an essential parameter in forming hexagonal nanoscale patterns on the surface of stainless steel.[31] Interestingly, we found that non-uniform etching of the Zr-4 sheet occurred after EP when platinum gauze was used as the counter electrode despite continuous electrolyte stirring (Fig. S1b and c†). Zr-4 surface facing towards the counter electrode (labelled as front surface) has a different finishing (Fig.-S1b†) compared to its opposite (back) surface (Fig. S1c†). A small black area can be seen clearly on the back surface of Zr-4 sheets (Fig. S1c†) compared to the front surface.

The reason behind this is the non-uniform electric field distribution due to the difference in the distance between the

Table 2 Electropolishing conditions of Zr-4 sheets

Electrolyte	Voltage (V)	Bath temperature (°C)	Time (s min^{-1})
Methanol–perchloric acid (4 : 1)	5 V	−1 °C	1.0 min 1.5 min 3.0 min
Methanol–perchloric acid (4 : 1)	10 V	−1 °C	30 s 1.0 min
Ethylene glycol monobutuly ether–perchloric acid (19 : 4)	50 V	−5 °C	30 min

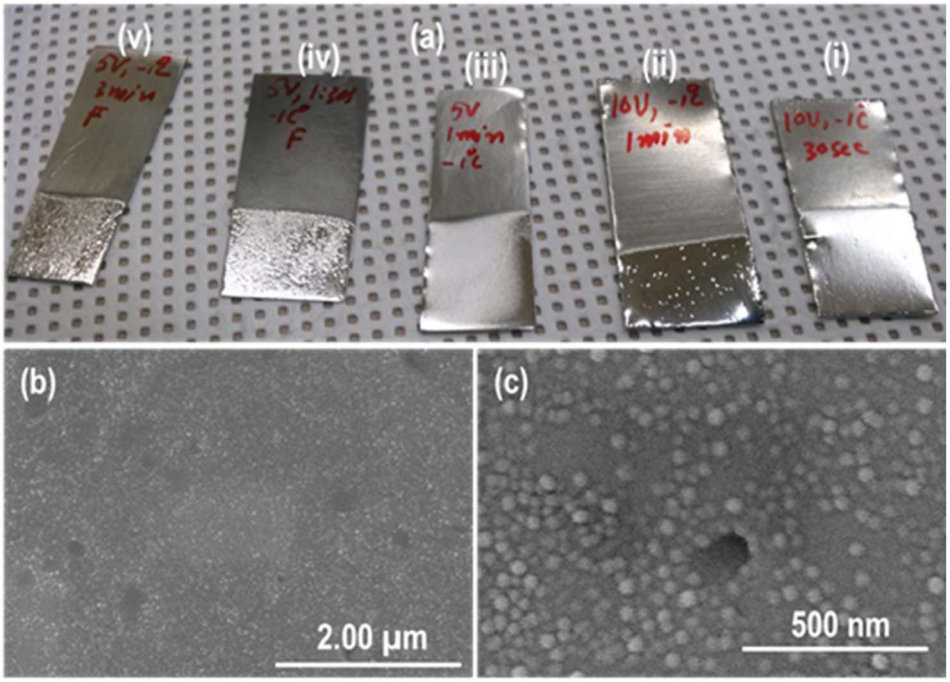

Fig. 2 (a) Digital picture of the electropolished Zr-4 sheet in methanol–perchloric acid (EP-MeOH-5V-1min, EP-MeOH-10V-30s, EP-MeOH-10V-1min, EP-MeOH-10V-3min), (b and c) FESEM images showing the morphology of the electropolished Zr-4 sheet.

electrode's surfaces. It has been reported that the resulting morphology produced on the anode (working electrode) surface is affected by various parameters, including electric field distribution.[42] Using the commercial code (COMSOL), we reported in our previous article that the electric field around the anode surface is not uniform during the anodization process.[16] It was found that the electric field near the anode (Zr-4) surface facing toward the cathode (front surface) is always different from the electric field existing near the opposite (labelled as back surface) surface of the anode. As a result, non-homogeneous itching and, hence, morphology are produced on both anode surfaces after anodization. A uniform electric field around Zr-4 samples was obtained by employing a specially designed counter electrode and simulating the electric field distribution during anodization using COMSOL.[16,43] Therefore, a simple copper (Cu) counter electrode in the form of a wire with an O-ring shape was designed for uniform electric field generation (Fig. S2a†). A digital picture of the front and back sides of Zr-4 sheets electropolished in methanol–perchloric acid using the Cu electrode is shown in Fig. S2b and c.† Zr-sheets's front and back surfaces exhibit a smooth and uniform finish without any black area formation. The EP produced an extraordinarily smooth and clean surface and reduced the roughness tremendously compared to MP (MP-4000-45 min), as evident from the FESEM images (Fig. 2b and c). The grains formed after MP with visible grain boundaries were not observed in the Zr-4 sheet after EP. Residual-like small spherical nanoparticles formed on the surface of Zr-4 after EP, whose nature is unknown. Recently, we have discovered that when Sus-304L was electropolished under optimized conditions in ethylene glycol monobutyl ether–perchloric acid electrolyte, a honey-comb-like hexagonal shallow nanoscale pattern was generated.[35] Therefore, the Zr-4 sheet was electropolished in the same electrolyte under similar conditions (see Table 2 for details) to form nanoscale patterned morphology similar to Sus-304L. EP parameters were selected based on the results obtained in our previous work on Sus-304L. A diffused shiny and bright surface of the Zr-4 sheet was obtained after EP, as shown in the digital picture (Fig. 3a).

FESEM images (Fig. 3b and c) clearly show the formation of a novel and unique honey-comb-like hexagonal and highly-ordered patterned morphology of shallow nanopores on Zr-4 surface only with EP like Sus-304L. The shallow nanopores are arranged in hexagonal order with an average diameter of $\sim 35 \pm 2$ nm. This nanoscale patterned morphology is much better regarding smoothness, high degree, and long-range ordering than the one reported in our previous article after the dissolution of the Zr-4 oxide layer formed during the first-step anodization.[14] This shows that the nanopattern produced on the Zr-4 surface during EP is superior to that obtained using the conventional method of oxide layer dissolution in solvent (water/ethanol) *via* ultra-sonication, leading to pattern distortion and sample damage. This phenomenon was confirmed when the bottom surface of the Zr-4 oxide layer was analyzed using FESEM after its detachment from the Zr-4 substrate, revealing a rough surface morphology of the Zr-4 oxide nanotube at the bottom surface.[14] Based on the present study, we found that EP of the Zr-4 sheet in ethylene glycol monobutyl ether–perchloric acid electrolyte produces excellent results. Previously, we have explored various anodic morphologies of the Zr-4 in organic electrolytes under different anodizing conditions and investigated its anti-corrosion properties in different environments.[13–16,36] However, this is the

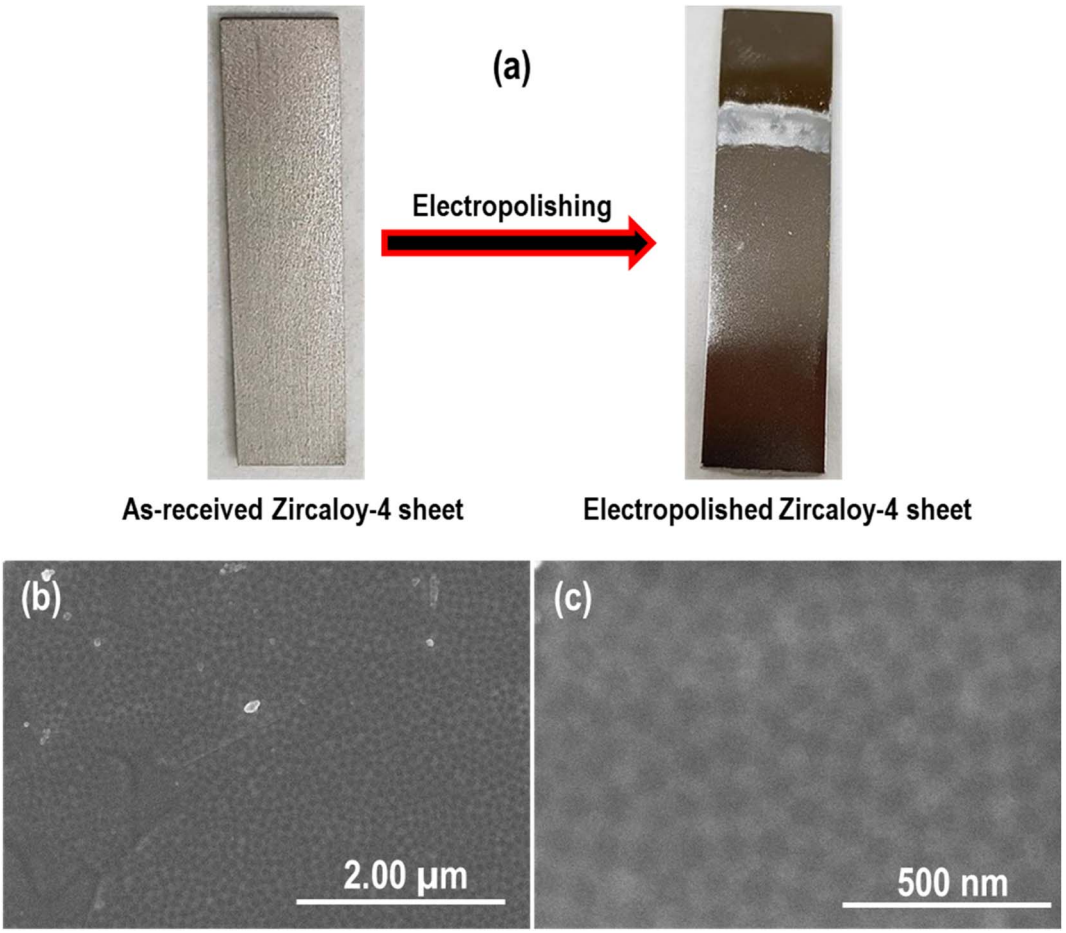

Fig. 3 (a) Digital picture of the as-received and electropolished Zr-4 sheet in ethylene glycol monobutyl ether–perchloric acid (EP-EG-50V-3°C-30min, EP-EG-50V-3°C-1min) (b and c) FESEM images showing the formation of a novel nanoscale patterned morphology on the surface of Zr-4 sheet after EP.

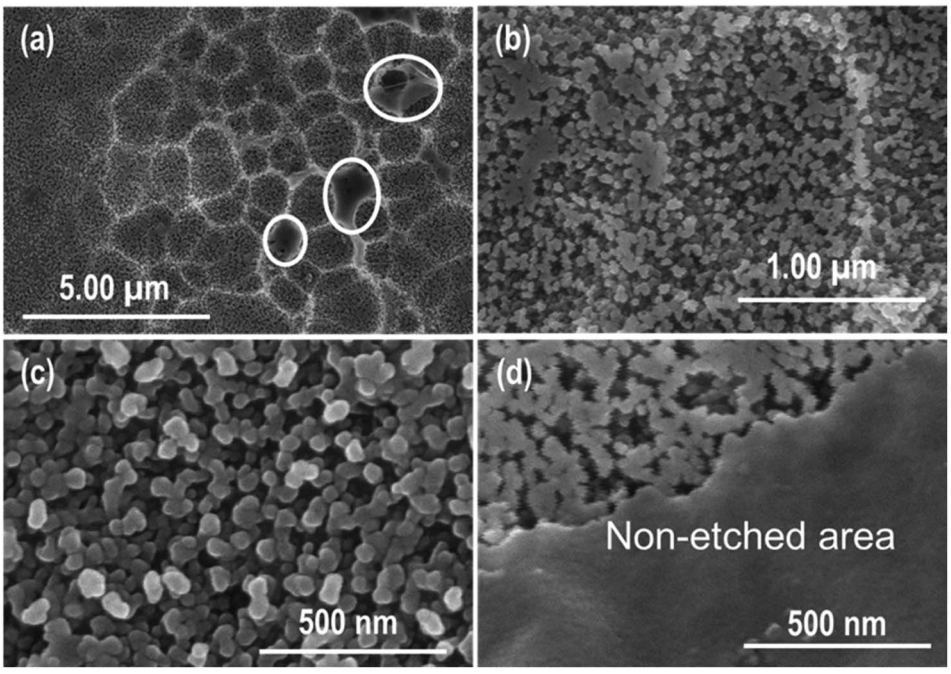

Fig. 4 FESEM images showing the morphology evolved on the surface of Zr-4 due to chemical polishing for 3 min in HF : HNO_3 : H_2O electrolyte (CP-3min-HFHNO$_3$). (a and b) Low magnification images reveal the formation of grain boundaries, (c) high magnification images exhibit the formation of nanostructure inside the grains, and (d) high magnification images show the un-etched area of the Zr-4 sheet.

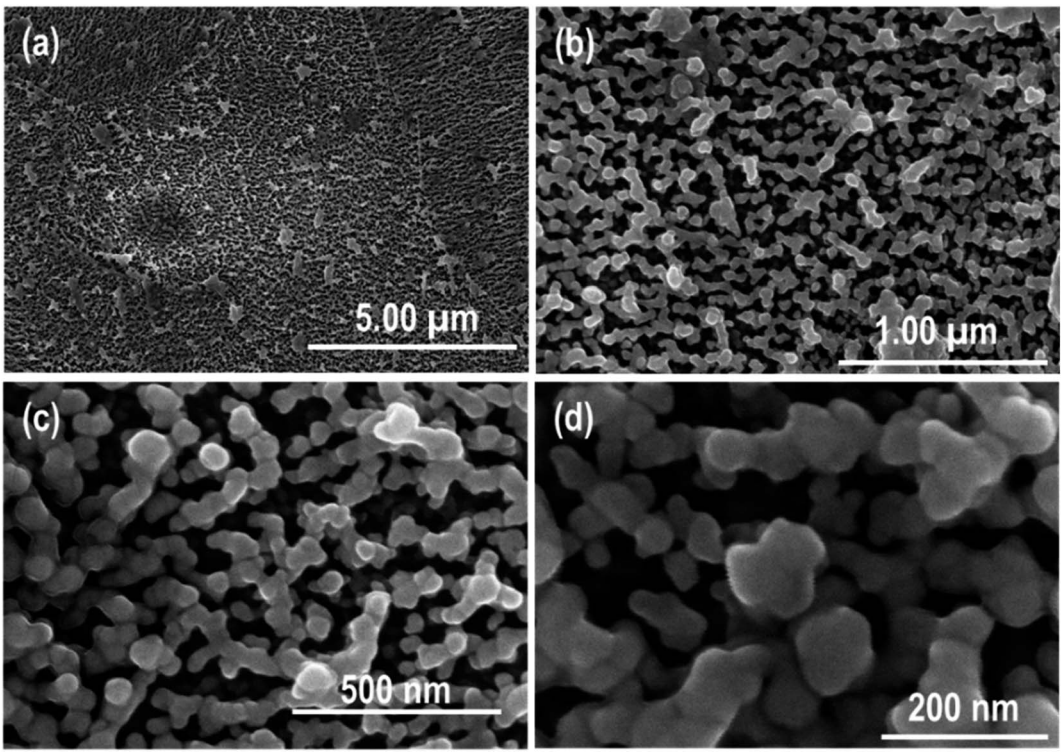

Fig. 5 FESEM images showing the morphology produced on the surface of Zr-4 as a result of chemical polishing for 5 min in HF : HNO_3 : H_2O electrolyte (CP-5min-$HFHNO_3$) (a and b) low magnification images revealing the formation of columnar morphology, (c and d) high magnification images exhibiting the formation of nanostructure.

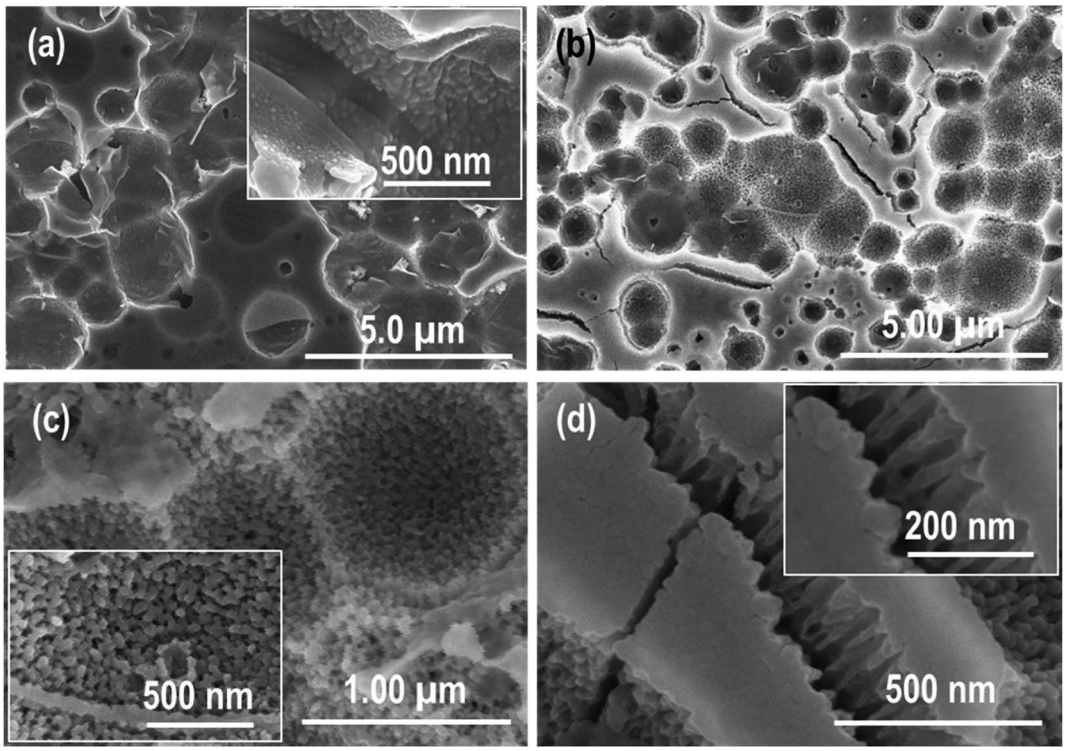

Fig. 6 FESEM images showing the morphology evolved on the surface of Zr-4 after (a) CP for 30 seconds, (b) low magnification image revealing the formation of cracks after anodization in glycerol-based electrolyte at 50 V for 2 h, (c) high magnification image exhibiting the formation of nanostructure inside the grains, (d) high magnification image showing the formation of nanotube (inset image) in the un-etched area.

first study to report the generation of novel nanopatterned on the surface of Zr-4 using only electrochemical polishing. This study is fascinating and unique because the formation of hexagonal nanoscale patterned has, until now, only been reported for stainless steel.[30–32,35] The findings from the studies on Zr-4 and Sus-304L reveal that the formation of honeycomb-like hexagonal nanopatterns is independent of the material nature and primarily depends on the electrolyte, as the two alloys have different compositions. This hypothesis is also consistent with the literature on stainless steel, where the patterned morphology was mainly found in the same electrolyte.[30–32,35] Therefore, this investigation will open new possibilities for other alloys and valve metals to achieve hexagonal nanoscale patterned morphology using only EP (EP-EG-50V-3°C-30min, EP-EG-50V-3°C-1min).

The possible mechanism of hexagonal nanopatterned formation on the surface of Zr-4 can be explained based on the electrolyte used for EP. We noted that the mechanism presented in this study is similar to the one reported in the case of stainless steel EP in such aspects as the nature of the electrolyte, EP conditions, and formation and dissolution of the as-grown oxide layer. Previously, we proposed a possible mechanism for the formation of shallow nanoscale patterned morphology on the surface of Sus-304L based on the change in the electrolyte color. The hexagonal and highly-ordered nanopattern was obtained as a result of the simultaneous formation and dissolution of the growing oxide layer from the electrolyte color change before and after EP in ethylene glycol monobutyl ether–perchloric acid electrolyte.[35] It has also been reported that methanol played a key role in the growing oxide layer destabilization by weakening the physical bond strength between the growing oxide layer and its substrate. Perchloric acid plays a dual role during the EP process. It facilitates the dissolution of the oxide layer due to the action of perchlorate ions, which aggressively attack and detach the oxide layer from the substrate. At the same time, perchloric acid favors the ionization of Zr-4 atoms, suppressing oxide formation due to its low pH environment enriched with H^+ ions. This controlled oxide layer formation and dissolution mechanism is essential for

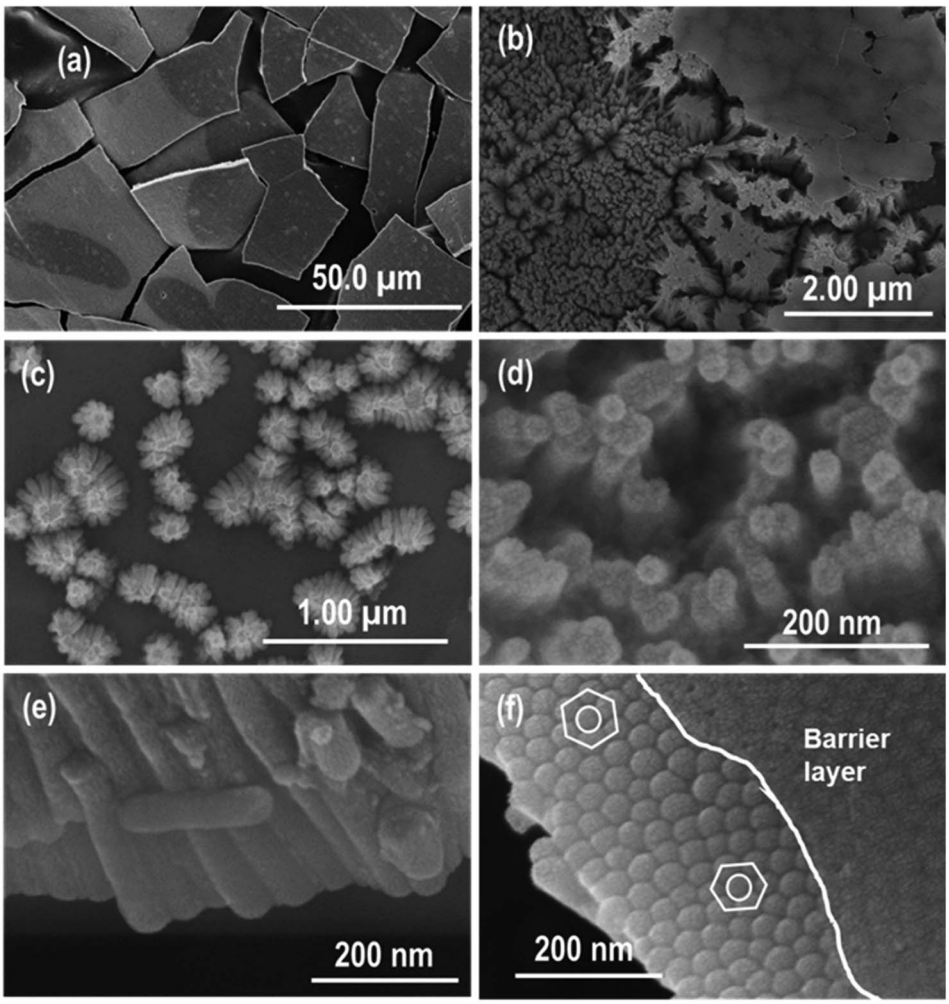

Fig. 7 FESEM images showing the morphology generated on the surface of Zr-4 after anodization of mechanical polished Zr-4 samples in glycerol-based electrolyte at 50 V for 2 h, (a and b) low magnification images revealing the formation of many cracks after sonication, (b) low magnification image exhibiting the formation of topmost thin oxide layer, (c and d) images showing the detachment of Zr-4 oxide nanotubes after sonication, (e) area of the bottom of the Zr-4 oxide layer revealing the formation of nanotube with close end, (f) bottom surface showing the formation of thin barrier layer on the bottom surface.

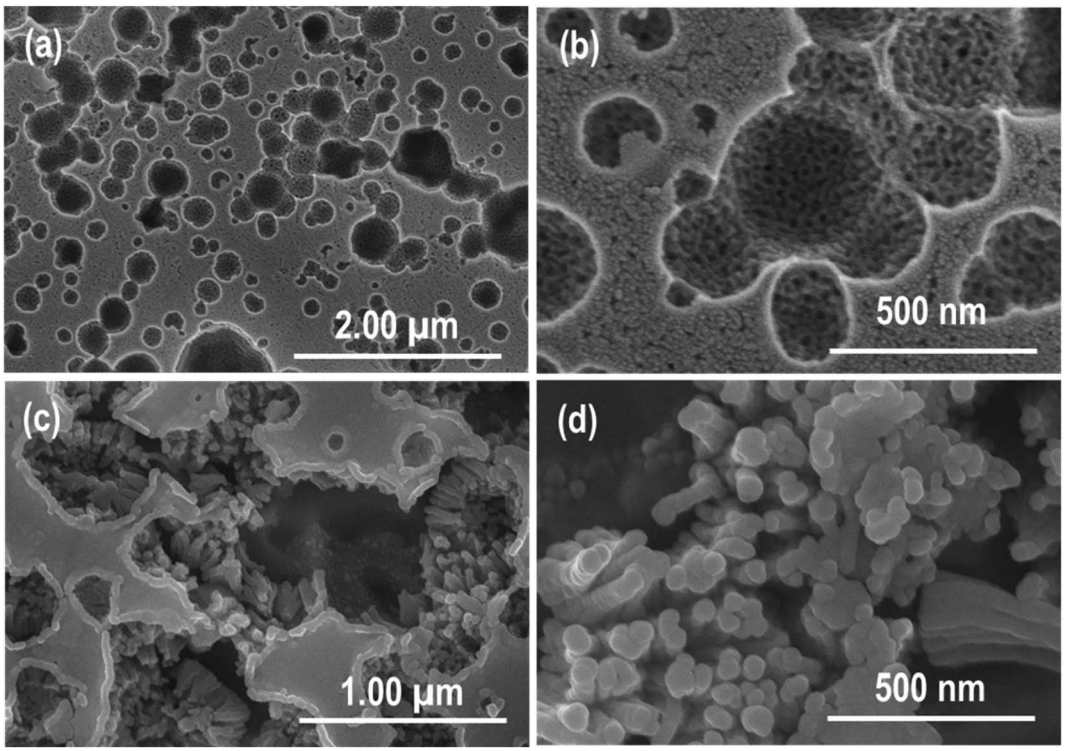

Fig. 8 FESEM images showing the morphology produced on the surface of mechanically–chemically polished Zr-4 sheet after anodization in the glycerol-based electrolyte at 50 V for 2 h, (a) low magnification showing the formation of voids as a result of chemical etching, (b) high magnification image showing the formation of nanostructure inside voids/grains, (c and d) sonication in water reveals the formation of nanotubes which are converted into nanorods and detached from Zr-4 substrate after sonication.

promoting patterning.[41,44] The role of the ethylene glycol monobutyl ether is equally important. The high viscosity of ethylene glycol monobutyl ether slows down the mass transport during EP. In this regime, the reaction becomes controlled by mass transport, which is a critical factor for achieving a smooth surface and brightening conditions conducive to nanopattern formation. Peighambardoust and Nasirpouri observed the formation of an oxide layer at the Ti surface after EP for a short time in the mixture of perchloric acid–methanol–ethylene glycol electrolyte. The formed oxide layer was dissolved with increased EP timing, producing a smooth surface finish.[41] In addition, they also found that EP at high voltage (25 V) led to the dissolution of the oxide layer at the onset of the experiment. Reggiani *et al.* also observed the formation and dissolution of the oxide layer many times on the Ti surface during EP in methanol–perchloric acid electrolyte.[44] Similarly, Schmuki *et al.* obtained a layered TiO_2 nanotubular structure in powder after Ti anodization in a perchlorate solution.[45] Hence, it can be deduced that perchloric acid is vital for forming and dissolving the oxide layer due to perchlorate ions, which attack the growing oxide layer and detach it from the substrate. However, the formation of a honeycomb-like hexagonal nanoscale pattern on the surface of Zr-4 cannot be solely attributed to the role of perchloric acid, as this morphology is not achieved in a methanol–perchloric acid electrolyte. This raises an open question for further debate. The role of ethylene glycol monobutyl ether cannot be ignored, as patterned morphology on the surface of stainless steel was predominantly obtained after EP in ethylene glycol monobutyl ether-based electrolytes.[30–32,35] It is a well-known fact that ethylene glycol and glycerol-based organic electrolytes are extensively employed for the anodization of metals and alloys after the breakthrough work of Schmuki.[46] Therefore, we can postulate that Zr-4 oxide layer is formed and simultaneously etched during EP in ethylene glycol monobutyl ether–perchloric acid electrolyte and leaves behind the footprint as a hexagonal nanoscale pattern. Further, work on the valve metals and alloys electropolishing is in progress, and we are trying to find the exact reason for patterned formation with some experimental evidence.

3.3 Chemical polishing effect on the Zr-4 morphology before anodization

To study the effect of CP on Zr-4 surface morphology before anodization, the electropolished samples were immersed in $HF : HNO_3 : H_2O$ electrolyte for different time intervals (the samples are represented as CP-3min-$HFHNO_3$ and CP-5min-$HFHNO_3$). Zr-4 sheet dipping for 3 min generated a unique and completely different morphology of random nanopores (Fig. 4). The grain boundaries are visible in the low-magnification images (Fig. 4a and b). The high magnification image (Fig. 4c) shows the inner grain structure, which reveals the formation of small and dense nanoparticles with porosity, adhered strongly to the Zr-4 surface. Some regions in the Zr-4 sheet remain completely un-etched, as shown in the images (marked areas of

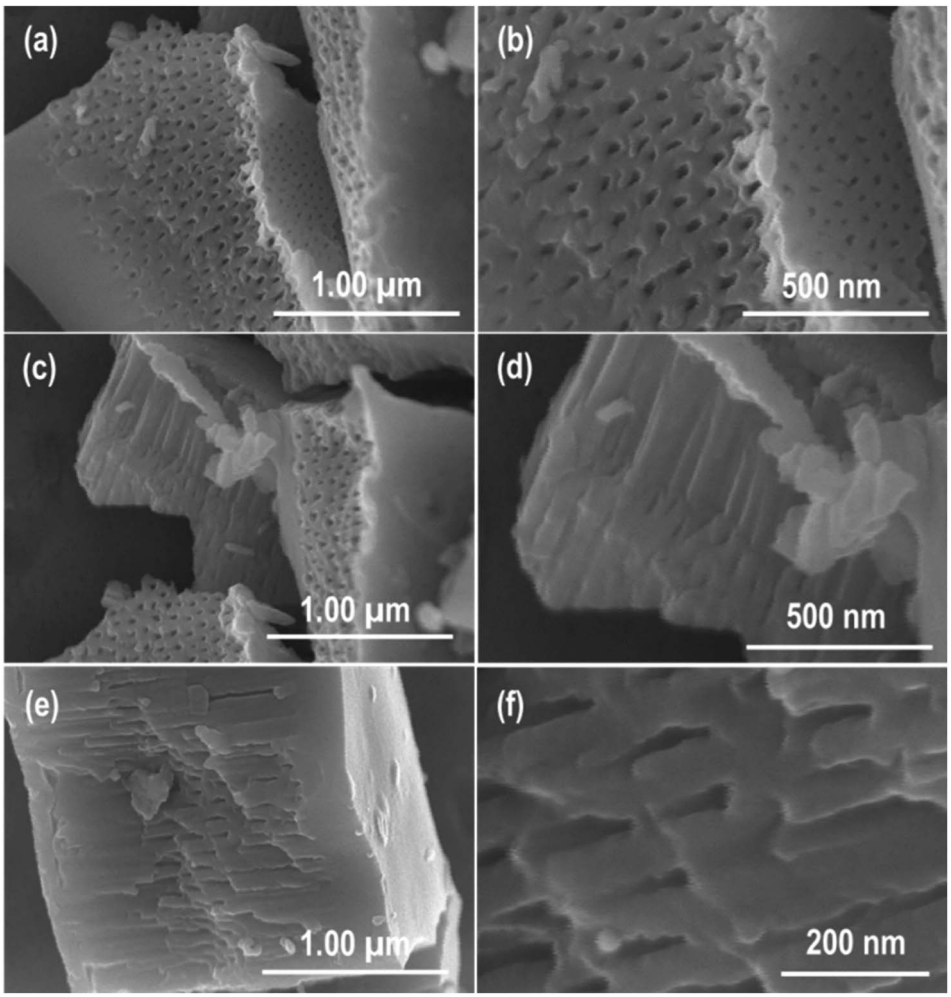

Fig. 9 FESEM images of the electropolished Zr-4 sheet after anodization in glycerol-based electrolyte at 50 V for 2 h, showing the formation of hybrid nanostructure (a and b) top surface image showing the formation of ordered nanopores with different diameters, (c and d) showing the formation of nanopores at the top surface while nanotubes near the bottom surface, (e and f) SEM image near bottom revealing the formation of nanotubes.

Fig. 4a and d). Further increase in the CP time to 5 min completely vanished the grains boundaries, and the morphology of the grains with enhanced porosity evolved (Fig. 5). The particulate morphology, obtained previously with a short etching time, slightly changed to a columnar structure with increased CP timing. These images also reveal that the pores become more profound and broader with enhanced porosity compared to Fig. 4 due to the relatively longer etching time. Still, a few tiny un-etched regions can be seen in a minimal area, as shown in Fig. 5a. These results reveal that the smooth surface morphology of the Zr-4 sheet obtained after EP in methanol–perchloric acid electrolyte is transformed into a porous particulate morphology with CP.

4. Polishing effect on anodic Zr-4 surface

4.1 Chemical polishing effect on the anodic Zr-4 surface

The relatively smooth surface of the as-received Zr-4 sheet was transformed into grains and voids formation after CP for 30 seconds in $HF : HNO_3 : H_2O$ electrolyte due to the preferential chemical etching (Fig. 6a). Numerous voids and grains of different sizes were formed whose boundaries can be seen clearly. To study the effect of CP on anodic Zr-4 nanostructure, anodization of the chemically polished sample was carried-out in glycerol-based electrolyte at 50 V for 2 h at room temperature. FESEM result (Fig. 6b) shows that almost the same grains and voids structure morphology is retained even after anodization with more clarity than Fig. 6a. The high magnification image of the grain (Fig. 6c) reveals the formation of particulate morphology similar to one observed after CP of the electropolished Zr-4 sample shown in Fig. 4. This indicates that this morphology remains relatively stable even after anodization. The formation of cracks in the non-etched regions can also be seen (Fig. 6d), which can be attributed to the volume expansion due to anodization.[25] The high magnification image of the cracked region exhibits the formation of Zr-4 oxide nanotubes beneath the top oxide layer (inset image in Fig. 6d). These nanotubes are observed only in the non-etched regions of the sample. This result shows that a mixture of nanotubular and

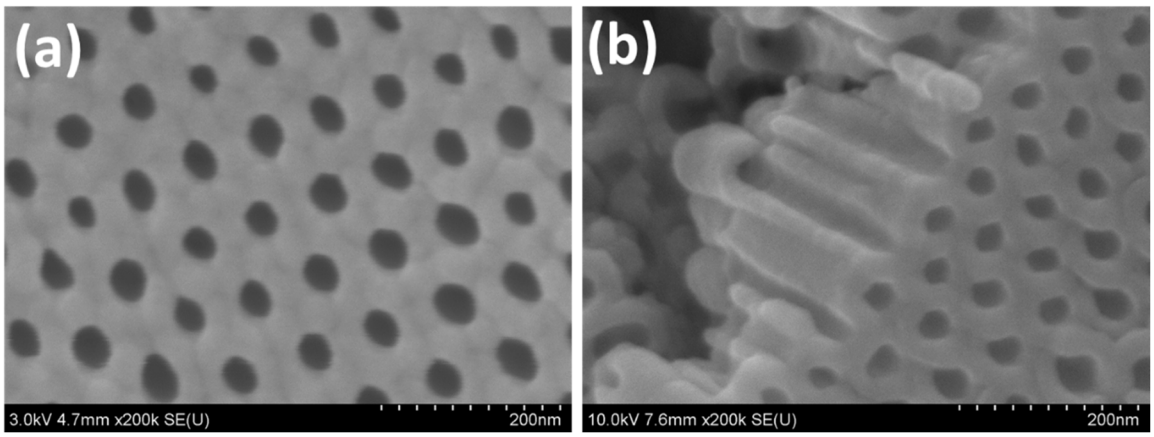

Fig. 10 FESEM images of the electropolished and anodized Zr-4 sample showing the (a) top surface view, (b) cross-sectional view of the Zr-4 oxide nanotubes.

particulate structures is formed due to the anodization of the chemically polished Zr-4 sample.

4.2 Mechanical polishing effect on the anodic Zr-4 surface

The mechanically polished Zr-4 samples anodized in the glycerol-based electrolyte at 50 V for 2 h resulted in the formation of an oxide layer on its surface, as shown in Fig. 7. The entire oxide layer becomes cracked into small pieces during the sample preparation for SEM characterisation and sonication in water for 2 min (Fig. 7a). The top surface view at low magnification shows that after sonication, the uppermost thin, compact oxide layer is dissolved from some regions besides bundling of the nanotubes (Fig. 7b). Crack formation is also visible in the uppermost oxide layer. Sonication dissolved the uppermost thin oxide layer and removed the thick nanotubular oxide layer from the substrate in some areas, as seen in Fig. 7c. The magnified image shows that the opening (mouth) of the nanotubes is blocked due to the oxide layer dissolution due to water sonication (Fig. 7d). Fig. 7e reveals that the opening of the nanotubes is not only blocked at the top surface but also near the bottom surface. This result shows that the dissolution of nanotubes occurred throughout their entire length. The bottom surface (Fig. 7f) shows a hexagonal-closed-packed morphology with an average diameter of the nanotube ~35 nm. The nanotubes are closed at the bottom surface and possess a high degree of ordering. A thin barrier layer can be seen, which covers the nanotubes at the bottom surface. We also studied the effect of CP on the surface morphology of the mechanically polished Zr-4 sheet. Therefore, the mechanically polished Zr-4 sample was first chemically polished under similar conditions in the aforementioned electrolyte and then anodized in the glycerol-based electrolyte at the same conditions for morphology comparison. Fig. 8 shows FESEM images of the mechanically polished Zr-4 sample after chemical polishing and anodization. Preferential attack (etching) of the chemicals on the Zr-4 sheet produced voids and grains, as shown in the low magnification image (Fig. 8a). These voids and grains are almost similar to the ones created on the surface of the chemically polished Zr-4 sheet (Fig. 6). The high-magnification image (Fig. 8b) reveals the formation of nanotubular structures inside the grains. Sonication in water for 2 min was carried out to unfold the top surface morphology. FESEM images show that sonication broke out the uppermost thin oxide layer and revealed the formation of nanotubes beneath it (Fig. 8c and d). Moreover, sonication in water detached the nanotubes from the Zr-4 substrate and dissolved them, besides the bundling issue, as observed previously. Additionally, the openings of the nanotubes observed in the voids (Fig. 8b) become closed after sonication (Fig. 8d). This result shows that sonication of Zr-4 oxide nanostructure in water changes the morphology of the oxide layer from nanotubes to nanorods. Therefore, in a two-step anodization process, sonication in water is useful for removing the oxide layer formed during the first-step anodization.

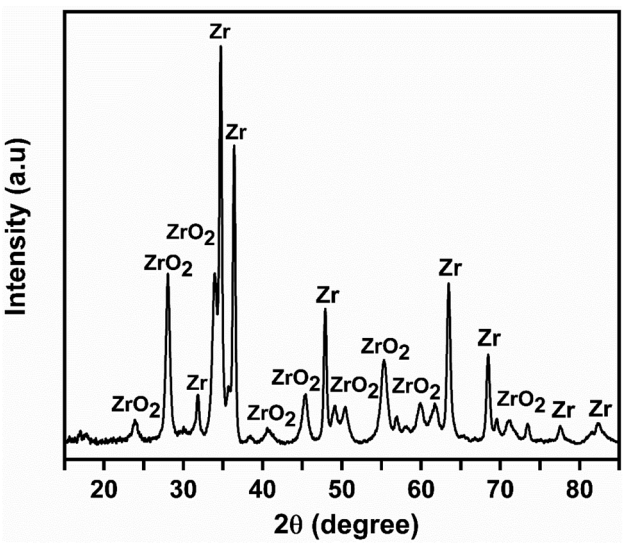

Fig. 11 XRD pattern of the electropolished and anodized Zr-4 sheet annealed at 450 °C for 2 h confirming the formation of Zr-4 oxide layer.

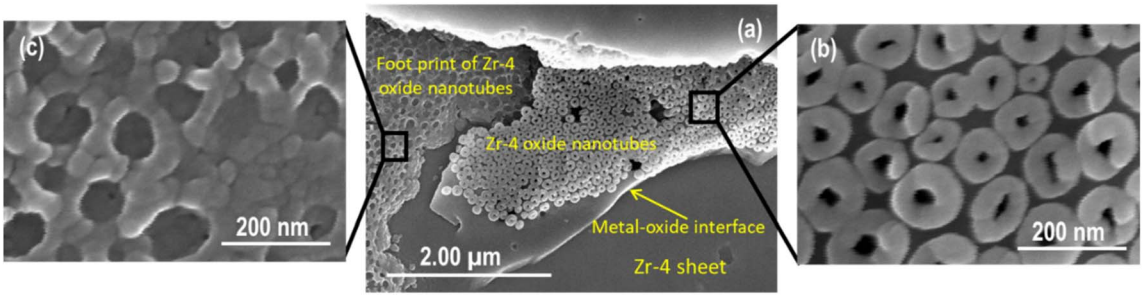

Fig. 12 FESEM images showing the (a) area near the metal-oxide interface in the Zr-4 substrate, (b) formation of Zr-4 oxide nanotubes with spacing, (c) foot pattern of Zr-4 oxide nanotubes after detachment as a result of sonication.

4.3 Electropolishing effect on the anodic Zr-4 surface

Upon anodizing the electropolished sample in glycerol-based electrolyte under similar conditions, a unique hybrid morphology of nanoporous structure at the top and nanotubular structure near the bottom surface was achieved. This type of hybrid morphology has been reported on the surface of Ti after the first-step anodization in used electrolyte.[47] Fig. 9 shows the top and cross-sectional surface view of the hexagonal patterned morphology (electropolished surface) anodized in glycerol-based electrolyte at 50 V for 2 h at room temperature. The top surface view of the anodic Zr-4 surface shows the formation of nanopores (Fig. 9a and b). This can be attributed to generating homogeneous and smooth hexagonal patterned morphology of shallow nanopores on the surface of Zr-4 after EP. The hybrid nanostructure formed *via* anodization of the nanopattern Zr-4 sample consisting of nanopores and nanotubes demonstrates significant potential for enhancing corrosion resistance and heat transfer efficiency in nuclear power reactors. As reported earlier, the patterned morphology protects the oxide layer from dissolution at the top surface during subsequent anodization.[35,39,40] A visible variation in the diameter of these nanopores was observed from the top surface toward the bottom surface (Fig. 9b). The diameter of the nanopores is smaller at the top surface than the diameter of the nanopores near the bottom surface. In our previous work on Sus-304L, the hexagonal and highly-ordered nanopattern production was due to the simulation's formation and dissolution of the oxide layer during EP. The cross-sectional morphology was investigated to check whether a complete nanoporous morphology was obtained on Zr-4 surface as the result of patterned morphology anodization. Fig. 9c and d reveals the simultaneous formation of nanopores and nanotubes contrary to the Sus-304L, where only a nanoporous morphology was obtained. It exhibits that nanopores are produced only at the top surface while nanotubes are near the bottom surface. The high-magnification image (Fig. 9d) clearly shows the formation of tubes near the bottom surface with closed-packed morphology. The cross-sectional images shown in Fig. 9e and f mostly reveal the formation of nanotubes across the Zr-4 anodic oxide layer. High-resolution SEM images of the electropolished and anodized Zr-4 sample near the top surface are given in Fig. 10. It shows the formation of hexagonal and highly-ordered nanopores with an average pore size of around 35 ± 2 nm. These results confirm the formation of a hybrid anodic Zr-4 nanostructure comprising nanopores at the top surface and nanotubes beneath it. This contrasts with the one we reported for Sus-304L, where a complete nanoporous structure morphology was obtained when the hexagonal patterned morphology was anodized in glycerol-based electrolyte. However, this type of hybrid morphology has been reported on the surface of Ti after the first-step anodization in residue electrolyte.[47]

The XRD pattern in Fig. 11 of the electropolished and anodized Zr-4 sample (annealed at 450 for 2 h) reveals the formation of an oxide layer (ZrO_2). It shows the peak of the Baddeleyite ZrO_2 phase (ICDD Card # 00-037-1484) along with peaks of the Zr-4 substrate (ICDD Card # 00-005-0665). Fig. 12 shows FESEM images of the Zr-4 sample near the metal-oxide interface. Zr-4 anodic nanotubes with non-uniform diameters, wall thickness, and different gaps can be seen (Fig. 12a). The foot-print morphology of Zr-4 oxide nanotubes (Fig. 12b), obtained as a result of detachment from the Zr-4 sheet due to sonication, is well matched with the external diameters of the nanotubes (Fig. 12c).

5. Conclusion

In summary, different polishing methods, such as chemical, mechanical, and electropolishing, and their combination, were employed on Zircaloy-4 sheets before and after anodization to investigate its effect on morphology. A few minutes of CP of the electropolished Zr-4 sheet in $HF : HNO_3 : H_2O$ generated a particulate morphology due to the preferential chemical attack. The particulate morphology transformed into a columnar structure with increased CP timing. EP of Zr-4 sheets under optimized conditions in ethylene glycol monobutyl ether–perchloric acid generated a novel hexagonal and high-ordered nanopatterned morphology. Subsequent anodization of the patterned morphology in glycerol-based electrolytes produced a unique hybrid nanostructure comprising nanopores and nanotubes. Anodization of the mechanically polished samples in glycerol-based electrolyte produced only nanotubular morphology. FESEM results revealed that the anodic Zr-4 nanotubes are transformed into nanorods after sonication in water due to Zr-4 oxide layer dissolution. The

results of this study indicate that electropolishing, which is facile and economical compared to the expensive and complicated pre-texturing techniques, could be applied to other alloys and valve metals to create hexagonal nanoscale patterns to protect materials from dissolution.

Data availability

All data generated and characterized during this study are included in the manuscript and ESI.†

Conflicts of interest

The authors declare that they have no competing interests.

Acknowledgements

This work was supported by the Innovative Small Modular Reactor Development Agency grant funded by the Korea government (Grant Number 00405419). The authors also acknowledge the financial support extended by the Researchers Supporting Project number (RSP2025R242), King Saud University, Riyadh, Saudi Arabia, for funding this research work.

References

1 B. Zhou and K. Feng, Zr–Cu alloy filler metal for brazing SiC ceramic, *RSC Adv.*, 2018, **8**(46), 26251–26254.
2 Y. J. Park, J. W. Kim, G. Ali and S. O. Cho, Enhancement of oxidation resistance of zirconium alloy with anodic nanoporous oxide layer in high-temperature air/steam environments, *Corros. Sci.*, 2018, **140**, 217–222.
3 S. Chatterjee, M. S. Fujimoto, N. L. Canfield, M. R. Elmore, D. W. Olson, E. C. Buck, *et al.*, An electrochemical technique for controlled dissolution of zirconium based components of light water reactors, *RSC Adv.*, 2019, **9**(4), 1869–1881.
4 C. Liu, G. Li, F. Yuan, F. Han, Y. Zhang and H. Gu, Stacking faults in Zr(Fe, Cr)$_2$ Laves structured secondary phase particle in Zircaloy-4 alloy, *Nanoscale*, 2018, **10**(5), 2249–2254.
5 H. Gu, G. Li, C. Liu, F. Yuan, L. Zhang, L. Wang, *et al.*, Characterization of the products obtained from the reactions of Zircaloy-4 with an acid mixture of concentrated HNO_3 and dilute HF with the aim of understanding pickle salts of zirconium alloys, *RSC Adv.*, 2016, **6**(111), 109815–109825.
6 K. Lee, A. Mazare and P. Schmuki, One-dimensional titanium dioxide nanomaterials: nanotubes, *Chem. Rev.*, 2014, **114**(19), 9385–9454.
7 C. Sousa, D. Leitao, M. Proenca, J. Ventura, A. Pereira and J. Araujo, Nanoporous alumina as templates for multifunctional applications, *Appl. Phys. Rev.*, 2014, **1**(3), 031102–031122.
8 W. Lee and S.-J. Park, Porous anodic aluminum oxide: anodization and templated synthesis of functional nanostructures, *Chem. Rev.*, 2014, **114**(15), 7487–7556.
9 G. Ali, H. J. Kim, J. J. Kim and S. O. Cho, Controlled fabrication of porous double-walled TiO_2 nanotubes *via* ultraviolet-assisted anodization, *Nanoscale*, 2014, **6**(7), 3632–3637.
10 R. Bose, S. P. Gajagouni, I. Barsoum, S. O. Cho and A. Alfantazi, Stainless steel-derived nano-porous oxide: a cost-efficient, stable, and corrosion-resistant hydrogen evolution catalyst, *J. Mater. Chem. A*, 2024, **12**(34), 22539–22549.
11 B. D. Mohapatra, K. Pawlik, I. Darowska, Ł. Gondek, M. Pisarek and G. D. Sulka, Understanding the morphological evolution of anodic tantalum oxide nanostructures in acidic medium, *Mater. Adv.*, 2024, **5**(16), 6560–6571.
12 A. Mozalev, Z. Pytlicek, K. Kamnev, J. Prasek, F. Gispert-Guirado and E. Llobet, Zirconium oxide nanoarrays *via* the self-organized anodizing of Al/Zr bilayers on substrates, *Mater. Chem. Front.*, 2021, **5**(4), 1917–1931.
13 G. Ali, Y. J. Park, H. J. Kim and S. O. Cho, Formation of self-organized Zircaloy-4 oxide nanotubes in organic viscous electrolyte *via* anodization, *Nanoscale Res. Lett.*, 2014, **9**, 1–7.
14 G. Ali, Y. J. Park, H. J. Kim and S. O. Cho, Compounds. Formation of hexagonally-ordered zircaloy oxide nanostructures with different morphologies using two-step anodization, *J. Alloys Compd.*, 2015, **640**, 205–209.
15 Y. J. Park, J. M. Ha, G. Ali, H. J. Kim, Y. Addad and S. O. Cho, Controlled fabrication of nanoporous oxide layers on zircaloy by anodization, *Nanoscale Res. Lett.*, 2015, **10**, 1–8.
16 Y. J. Park, J. W. Kim, G. Ali, H. J. Kim, Y. Addad and S. O. Cho, Fabrication of uniform nanoporous oxide layers on long cylindrical zircaloy tubes by anodization using multi-counter electrodes, *Nanoscale Res. Lett.*, 2017, **12**, 1–6.
17 D. H. Kam, H. S. Yu, Y. H. Jeong, Y. J. Park, J. W. Kim, S. O. Cho, *et al.*, CHF on Anodized Zirconium-based Alloy Surfaces with Protective Oxide Layers for ATF cladding, *Int. J. Heat Mass Transfer*, 2021, **170**, 120936.
18 W. Han and F. Fang, Fundamental aspects and recent developments in electropolishing, *Int. J. Mach. Tool Manufact.*, 2019, **139**, 1–23.
19 L. M. de Andrade, C. Paternoster, P. Chevallier, S. Gambaro, F. Copes, V. F. de Oliveira Sales, *et al.*, Electropolishing Fe-based biodegradable metals for vascular applications: impact on surface properties, corrosion and cell viability, *RSC Appl. Interfaces*, 2025, DOI: **10.1039/D4LF00113C**.
20 M. M. Taheri, B. Rezaee, H. Pakzad and A. Moosavi, Condensation heat transfer enhancement through durable, self-propelling fluorine-free silane-treated anodized surfaces, *J. Mater. Chem. A*, 2024, **12**(40), 27327–27339.
21 M. Abdallah, M. Hegazy, H. Ahmed, A. S. Al-Gorair, H. Hawsawi, M. Morad, *et al.*, Appraisal of synthetic cationic Gemini surfactants as highly efficient inhibitors for carbon steel in the acidization of oil and gas wells: an experimental and computational approach, *RSC Adv.*, 2022, **12**(27), 17050–17064.
22 W. Zhu, X. Li, X. Liu, L. Bai, X. Wang, A. Li, *et al.*, Enhancing the corrosion resistance of waterborne epoxy coatings with functionalized biochar, *RSC Adv.*, 2024, **14**(53), 39747–39758.

23 H. Sopha, T. Samoril, E. Palesch, L. Hromadko, R. Zazpe, D. Skoda, *et al.*, Ideally hexagonally ordered TiO_2 nanotube arrays, *ChemistryOpen*, 2017, **6**(4), 480–483.
24 T. Kondo, S. Nagao, S. Hirano, T. Yanagishita, N. T. Nguyen, P. Schmuki, *et al.*, Fabrication of ideally ordered anodic porous TiO_2 by anodization of pretextured two-layered metals, *Electrochem. Commun.*, 2016, **72**, 100–103.
25 S. Berger, J. Kunze, P. Schmuki, D. LeClere, A. T. Valota, P. Skeldon, *et al.*, A lithographic approach to determine volume expansion factors during anodization: Using the example of initiation and growth of TiO_2-nanotubes, *Electrochim. Acta*, 2009, **54**(24), 5942–5948.
26 J. Choi, R. B. Wehrspohn, J. Lee and U. Gösele, Anodization of nanoimprinted titanium: a comparison with formation of porous alumina, *Electrochim. Acta*, 2004, **49**(16), 2645–2652.
27 A. Rauf, M. Mehmood, M. Asim Rasheed and M. Aslam, The effects of electropolishing on the nanochannel ordering of the porous anodic alumina prepared in oxalic acid, *J. Solid State Electrochem.*, 2009, **13**, 321–332.
28 D. Ma, S. Li and C. Liang, Electropolishing of high-purity aluminium in perchloric acid and ethanol solutions, *Corros. Sci.*, 2009, **51**(4), 713–718.
29 A. Kityk, V. S. Protsenko, F. I. Danilov, O. Kun and S. A. Korniy, Electropolishing of aluminium in a deep eutectic solvent, *Surf. Coat. Technol.*, 2019, **375**, 143–149.
30 H. Tsuchiya, T. Suzumura, Y. Terada and S. Fujimoto, Formation of self-organized pores on type 316 stainless steel in organic solvents, *Electrochim. Acta*, 2012, **82**, 333–338.
31 F. Martin, D. Del Frari, J. Cousty and C. Bataillon, Self-organisation of nanoscaled pores in anodic oxide overlayer on stainless steels, *Electrochim. Acta*, 2009, **54**(11), 3086–3091.
32 V. Vignal, J. Roux, S. Flandrois and A. Fevrier, Nanoscopic studies of stainless steel electropolishing, *Corros. Sci.*, 2000, **42**(6), 1041–1053.
33 A. Seyeux, S. Berger, D. LeClere, A. Valota, P. Skeldon, G. E. Thompson, *et al.*, Influence of surface condition on nanoporous and nanotubular film formation on Titanium, *J. Electrochem. Soc.*, 2008, **156**(2), K17.
34 K. Lu, Z. Tian and J. A. Geldmeier, Polishing effect on anodic titania nanotube formation, *Electrochim. Acta*, 2011, **56**(17), 6014–6020.
35 A. Hassan, G. Ali, Y. J. Park, A. Hussain and S. O. Cho, Formation of a self-organized nanoporous structure with open-top morphology on 304L austenitic stainless steel, *Nanotechnology*, 2020, **31**(31), 315603.
36 Y. J. Park, J. W. Kim, G. Ali and S. O. Cho, Enhancement of oxidation resistance of zirconium alloy with anodic nanoporous oxide layer in high-temperature air/steam environments, *Corros. Sci.*, 2018, **140**, 217–222.
37 J. Li, X. Bai, D. Zhang and H. Li, Characterization and structure study of the anodic oxide film on Zircaloy-4 synthesized using NaOH electrolytes at room temperature, *Appl. Surf. Sci.*, 2006, **252**(20), 7436–7441.
38 C. Lee, H. Kim, H. S. Ahn, M. H. Kim and J. Kim, Micro/nanostructure evolution of zircaloy surface using anodization technique: Application to nuclear fuel cladding modification, *Appl. Surf. Sci.*, 2012, **258**(22), 8724–8731.
39 H. Ullah, F. Usman, M. A. Rasheed, A. A. Khan, R. Ahmad, S. Y. Lee, *et al.*, Anodic SnO_2 Nanoporous Channels Functionalized with CuO Quantum Dots for Selective H_2O_2 Biosensing, *ACS Appl. Nano Mater.*, 2022, **5**(7), 9096–9111.
40 H. Ullah, R. Ahmad, A. A. Khan, N. E. Lee, J. Lee, A. U. Shah, *et al.*, Anodic SnO_2 nanoporous structure decorated with Cu_2O nanoparticles for sensitive detection of creatinine: experimental and DFT study, *ACS Omega*, 2022, **7**(46), 42377–42395.
41 N. Peighambardoust and F. Nasirpouri, Electropolishing behaviour of pure titanium in perchloric acid–methanol–ethylene glycol mixed solution, *Trans. IMF*, 2014, **92**(3), 132–139.
42 L. Sun, S. Zhang, X. W. Sun and X. He, Effect of electric field strength on the length of anodized titania nanotube arrays, *J. Electroanal. Chem.*, 2009, **637**(1–2), 6–12.
43 S. Y. Lee, J. Lee, J. H. Lee, H. Y. Jeong and S. O. Cho, Direct conversion of aluminum wires into phase-controllable aluminum oxide nanoparticles by anodization for chromium adsorption, *ACS Appl. Nano Mater.*, 2021, **4**(3), 3108–3113.
44 R. C. Reggiani, F. Mazza and E. Sivieri, Electrochemical polishing of titanium in perchloric-methanolic solutions, *Mater. Chem.*, 1979, **4**(2), 149–158.
45 H. Jha, R. Hahn and P. Schmuki, Ultrafast oxide nanotube formation on TiNb, TiZr and TiTa alloys by rapid breakdown anodization, *Electrochim. Acta*, 2010, **55**(28), 8883–8887.
46 J. M. Macak, H. Tsuchiya, L. Taveira, S. Aldabergerova and P. Schmuki, Smooth anodic TiO_2 nanotubes, *Angew. Chem., Int. Ed.*, 2005, **44**(45), 7463–7465.
47 M. Hussain, N. Khaliq, A. A. Khan, M. Khan, G. Ali, M. Maqbool, *et al.*, Synthesis, characterization and electrochemical analysis of TiO_2 nanostructures for sensing l-Cysteine and hydrogen peroxide, *Phys. E*, 2021, **128**, 114541.